JOURNAL OF MATERIALS SCIENCE 22 (1987) 1758–1768

Formation, thermal stability and electrical resistivity of quasicrystalline phase in rapidly quenched Al–Cr alloys

AKIHISA INOUE, HISAMICHI KIMURA, TSUYOSHI MASUMOTO
The Research Institute for Iron, Steel and Other Metals, Tohoku University, Sendai 980, Japan

The icosahedral quasicrystal has been found to appear in a wide composition range from about 5 to 16 at% Cr in rapidly quenched Al–Cr alloys, but the formation of the quasicrystalline single phase was limited only in the vicinity of about 15.5 at% Cr. Analytical solute concentrations in the quasicrystalline phase are not always constant and increase continuously from 9.0 to 15.4 at% Cr with increasing nominal solute concentration from 6 to 15.4%. The quasicrystal can be approximately formulated to be $Al_{11}Cr_2$ with a maximum deviation of about 6% Cr from the stoichiometric ratio to lower concentration side. Vickers hardness and electrical resistivity increase gradually with increasing chromium content and rapidly at about 14.5% Cr, and their values of $Al_{84.6}Cr_{15.4}$ quasicrystal are 710 DPN, 2.38 $\mu\Omega$m at 4.2 K, and 2.72 $\mu\Omega$m at 293 K. On the other hand, the onset transformation temperature of quasicrystal to crystalline phase, T_t, and the heat of transformation, ΔH_t show maximum values of 644 K and 1805 J mol^{-1} at 14.5% Cr and decrease to 625 K and 550 J mol^{-1} at 15.4% Cr. $Al_{84.6}Cr_{15.4}$ quasicrystal transforms at two stages to a stable orthorhombic $Al_{11}Cr_2$ compound through a metastable intermediate phase with unidentified structure, while the quasicrystal + Al structure in Al–Cr alloys containing less than 15% Cr changes directly to stable phases of compounds and aluminium. The distinct difference in transformation behaviour of the quasicrystal is thought to be the reason for the abrupt changes in T_t and ΔH_t at a composition between 14.5 and 15.4% Cr.

1. Introduction

A quasicrystal with five-fold symmetry found in a rapidly quenched $Al_{85.7}Mn_{14.3}$ alloy [1] has attracted rapidly increasing interest as a new type of material, which does not belong to the two conventional categories of crystal and non-crystal. Almost all the studies on the formation range, structure, density, electrical and magnetic properties and thermal stability of Al-base quasicrystals have been focussed on Al–Mn [2–11] and Al–V [11, 12] systems. There is little information on the formation range and characteristics of quasicrystal in the other Al-base alloys. The clarification of the composition range, where Al-base quasicrystal is formed, is very important in understanding the mechanism of formation of quasicrystal during rapid cooling from liquid. The present authors found that the quasicrystal is formed in rapidly quenched Al–Cr alloys and the formation range of the quasicrystalline single phase is different from those of Al–Mn and Al–V quasicrystals. The aim of this paper is to clarify the formation range, internal defect structure, hardness, electrical resistivity, thermal stability and decomposition behaviour of the quasicrystal in rapidly quenched Al–Cr alloys and to investigate the difference in the formation tendency, structural features and characteristics among Al–Mn, Al–V and Al–Cr quasicrystals.

2. Experimental procedure

Al–Cr binary alloys containing 4, 6, 8, 10, 12.5, 14.5, 15.4, 16.5 and 18 at% Cr were used in the present work. The Al–Cr ingots were prepared by arc melting a mixture of pure aluminium (99.99 wt%) and chromium (99.75 wt%) in a purified argon atmosphere. The compositions of alloys reported are the nominal ones since the losses during arc melting were negligible. Rapidly quenched ribbon specimens with about 0.02 mm thickness and about 1 mm width were prepared from the pre-alloyed ingots under an argon atmosphere using a single roller melt spinning apparatus with a copper roller. The as-quenched and annealed structures were examined by X-ray diffractometer using Cu$K\alpha$ radiation, analytical transmission electron microscopy and differential scanning calorimetry. Thin foils for TEM were prepared by electrolytic polishing in an electrolyte of perchloric acid and ethanol with 1 : 9 volumetric ratio. TEM observation and microanalysis were performed on a JEM 200CX analytical microscope equipped with a Lind energy dispersive X-ray spectrometer (EDXS) with a Model 860 analyser system for standard-less analysis of the thin films. The electron microscopy (TEM/EDXS) analysis has been known to give microchemical distribution of constituent elements with an accuracy above ~0.5 to 1.0 at% [13], even though there are some

0022–2461/87 $03.00 + .12

unavoidable error factors such as surface thin film due to contamination, absorption and fluorescence effects of X-ray, limited accuracy of the standard-less analysis itself, etc. The details of the principle and technique have been described elsewhere [14]. Measurement of electrical resistivity was made by the DC method using the four-point probe technique in a wide temperature range from 4.2 to 293 K. The temperature was measured using a calibrated germanium thermometer at temperatures below about 90 K and a calibrated diode thermometer in the higher temperature range with accuracy better than ± 0.01 K and ± 0.1 K below and above 90 K, respectively. Hardness was measured by a Vickers microhardness tester with a 25 g load.

3. Results

3.1. Formation of the quasicrystal

Figs 1 and 2 show X-ray diffraction patterns as a function of diffraction angle for rapidly quenched $Al_{100-x}Cr_x$ (x = 4, 6, 8, 10, 14.5, 15.4 and 16.5%) alloys. Identification of the X-ray diffraction peaks corresponding to quasicrystal with an icosahedral structure was made by using six independent Miller indices as proposed by Bancel *et al.* [6]. As shown in Figs 1 and 2, the diffraction patterns consist of only fcc Al(Cr) solid solution at 4% Cr; quasicrystal + Al(Cr) in the range from 6 to 14.5% Cr; quasicrystalline single phase at 15.4% Cr; and quasicrystal + crystalline compound at 16.5% Cr. Figs 3a–d show selected area electron diffraction patterns of rapidly quenched $Al_{85.5}Cr_{14.5}$ alloy. Their patterns reveal

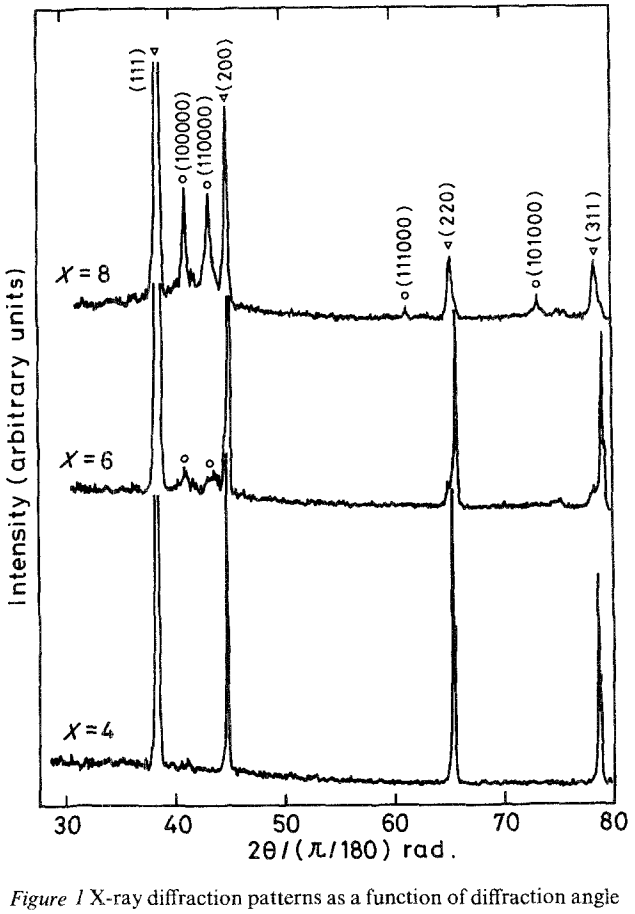

Figure 1 X-ray diffraction patterns as a function of diffraction angle for rapidly quenched $Al_{100-x}Cr_x$ (x = 4, 6 and 8 at %) alloys. ▽, Aluminium phase; ○, quasicrystalline phase.

TABLE I Analysis of X-ray diffraction pattern of the quasicrystalline phase in rapidly quenched $Al_{82.5}V_{17.5}$, $Al_{84.6}Cr_{15.4}$ and $Al_{77.5}Mn_{22.5}$ alloys

Index	Interlattice spacing (nm)		
	$Al_{82.5}V_{17.5}$	$Al_{84.6}Cr_{15.4}$	$Al_{77.5}Mn_{22.5}$
(111010)	0.3453	–	0.3324
(100000)	0.2252	0.2199	0.2164
(110000)	0.2125	0.2088	0.2056
(111000)	–	0.1515	0.1485
(101000)	0.1314	0.1293	0.1268

five-, three- and two-fold symmetries and can be identified to be $(100000)_q$, $(111000)_q$, $(110000)_q$ and $(112000)_q$, respectively, of icosahedral quasicrystal. These features are in good agreement with those of rapidly quenched $Al_{85.7}Mn_{14.3}$ alloy reported by Schechtman *et al.* [1]. It is particularly noticed that the quasicrystal single phase in rapidly quenched Al–Cr alloys appears in the vicinity of 15.4% Cr and the solute concentration for formation of the quasicrystal single phase is considerably lower than those (about 22% Mn and 20% V) for Al–Mn and Al–V alloys. This clearly indicates that the solute amount required to form a homogeneously quasicrystalline structure is not always constant for the Al–X (X = manganese, vanadium or chromium) alloys.

Table I summarizes interlattice spacings of the quasicrystalline phase determined from the X-ray diffraction pattern of rapidly quenched $Al_{84.6}Cr_{15.4}$ alloy, along with the data [11] for the quasicrystalline $Al_{77.5}Mn_{22.5}$ and $Al_{82.5}V_{17.5}$ phases. The interlattice spacings of the Al–Cr quasicrystal are located in the intermediate range of Al–Mn and Al–V alloys, and increase in the order of Al–Mn < Al–Cr < Al–V. It has previously been shown [11] that the difference in the interlattice spacings between Al–Mn and Al–V quasicrystals is attributed to the difference in packing fraction of Al–V and Al–Mn intermetallic compounds. Similarly, the difference of the interlattice spacings among Al–X (X = chromium, manganese or vanadium) quasicrystalline phases seems to be also interpreted by taking the packing fraction of Al–X intermetallic compounds into consideration. However, there are no data on crystal structure available to estimate the packing fraction of Al–Cr compounds and the packing fraction of Al–Cr compounds cannot be estimated. Here it appears important to point out that the interlattice spacings of the Al–X quasicrystalline phases have a strong correlation against the atomic size of each X element which is a simple parameter without consideration of bonding nature between atoms; the larger the atomic size the larger is the interlattice spacing of the quasicrystalline phases.

In order to clarify the change in microstructural features of the Al–Cr quasicrystals with chromium concentration, TEM observations were made for the rapidly quenched $Al_{100-x}Cr_x$ (x = 4 to 18 at %) alloys. As exemplified in Figs 4a–d, the area fraction occupied by the quasicrystalline phase increases continuously with increasing chromium content and $Al_{84.6}Cr_{15.4}$ alloy appears to consist only of quasicrystal, being in accordance with the results obtained by X-ray diffrac-

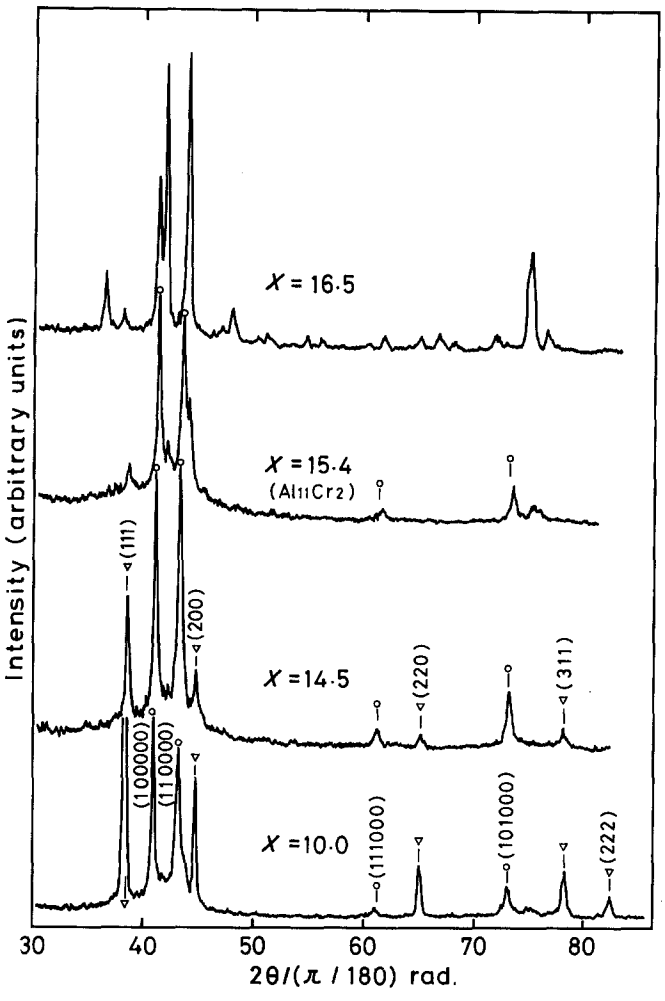

Figure 2 X-ray diffraction patterns as a function of diffraction angle for rapidly quenched $Al_{100-x}Cr_x$ (x = 10, 14.5, 15.4 and 16.5 at %) alloys. ▽, Aluminium phase; ○, quasicrystalline phase.

tion analysis. Additionally, it is seen in Fig. 4 that the morphology of the quasicrystal changes significantly in the vicinity of about 14 to 15% Cr, where the aluminium phase disappears almost completely. The quasicrystalline phase in Al–Cr alloys containing less than about 14.5% Cr is spherulitic in shape with a diameter of about 0.3 to 0.8 μm, and is characterized by radiating branches which stem from a central core. Also, the spherulite can be divided into subgrains with a size of about 0.1 to 0.2 μm. Additionally, the second phase with bright contrast corresponding to aluminium solid solution can be seen on the grain boundaries and subgrain boundaries. On the other hand, the quasicrystal in $Al_{84.6}Cr_{15.4}$ alloy consists of grains with a size of about 2 to 3 μm, and one cannot see radiating branches growing from a central core. The grain size of $Al_{84.6}Cr_{15.4}$ quasicrystal is about 2.5 to 10 times larger than that of Al–Cr alloys with chromium concentrations less than 14.5%, suggesting that the growth of the quasicrystal is much easier for a stoichiometric $Al_{11}Cr_2$ compound. No distinct change in the density of internal defects in the quasicrystalline phase is seen between $Al_{84.6}Cr_{15.4}$ and Al–Cr containing below about 14.5% Cr. Fig. 5 shows a rapidly quenched structure of $Al_{83.5}Cr_{16.5}$ alloy consisting of quasicrystal and orthorhombic $Al_{11}Cr_2$ compounds. The quenched structure is composed of equiaxed fine grains with a size of about 0.2 μm and the features of the morphology and internal defect structure are significantly different from those of Al–Cr alloys consisting of Al + quasicrystal duplex phases and a quasicrystalline single phase.

Table II summarizes aluminium and chromium compositions of transgranular quasicrystal and intergranular aluminium phases obtained by the EDXS method from a limited region smaller than about 80 nm in rapidly quenched $Al_{94}Cr_6$, $Al_{90}Cr_{10}$ and $Al_{84.6}Cr_{15.4}$ alloys. Here the previously reported data [11] of Al–Mn and Al–V quasicrystals are also presented for comparison. Additionally, typical examples of the EDXS spectrum taken from the quasicrystalline spherulite and intergranular aluminium phase in $Al_{90}Cr_{10}$ alloy are presented in Figs 6a and b. As seen in Table II and Fig. 6, the average chromium concentration in the quasicrystalline phase is 9.0% for $Al_{94}Cr_6$, 13.7% for $Al_{90}Cr_{10}$ and 15.4% for $Al_{84.6}Cr_{15.4}$, and that in the intergranular aluminium phase is 3.5% for $Al_{94}Cr_6$ and 1.2% for $Al_{90}Cr_{10}$. The systematic variation in the analytical chromium concentration in the quasicrystalline phase with nominal chromium content indicates that the nonequilibrium quasicrystalline phase can exist over a rather wide solute concentration of about 8.6 to 15.8% Cr. The solute concentrations are lower than 18.2 to 22.6% Mn [11] and 18.9 to 20.4% V [11] in Al–Mn and Al–V quasicrystals. From the analytical data, the composition of the Al–Cr quasicrystalline single phase can be approximately expressed as $Al_{11}Cr_2$, even though the stoichiometric ratio has a maximum deviation of about 6% Cr to lower concentration side. Table II

TABLE II Energy dispersive X-ray microanalytical concentration of transgranular quasicrystalline and intergranular aluminium phases in rapidly quenched Al–Cr alloys. The data for Al–Mn and Al–V quasicrystals were taken from [11]

Nominal composition of alloy (at %)	Analytical site	Analytical aluminium concentration (at %)	Analytical chromium concentration (at %)	Average analytical composition (at %)
$Al_{94}Cr_6$	Transgranular	90.4	9.6	$Al_{91.0}Cr_{9.0}$
		91.1	8.9	
		91.4	8.6	
	Intergranular	96.6	3.4	$Al_{96.5}Cr_{3.5}$
		96.5	3.5	
		96.3	3.7	
$Al_{90}Cr_{10}$	Transgranular	86.2	13.8	$Al_{86.3}Cr_{13.7}$
		85.7	14.3	
		86.2	13.8	
		88.0	12.0	
		85.7	14.3	
		85.8	14.2	
		86.9	13.1	
	Intergranular	98.9	1.1	$Al_{98.8}Cr_{1.2}$
		98.7	1.3	
		98.9	1.1	
$Al_{84.6}Cr_{15.4}$	Transgranular	84.7	15.3	$Al_{84.6}Cr_{15.4}$
		84.2	15.8	
		85.2	14.8	
		84.4	15.6	
		84.6	15.4	
		84.4	15.6	
$Al_{77.5}Mn_{22.5}$	Transgranular	77.4*	22.6*	$Al_{77.4}Mn_{22.6}$
$Al_{82.5}V_{17.5}$	Transgranular	79.6*	20.4*	$Al_{79.6}V_{20.4}$

*Average value.

also shows that the average solute concentration in the intergranular aluminium phase is about 1.2 to 3.5% Cr, being different from 6.7% Mn for Al–Mn alloys, and 2.1% V for Al–V alloys. The solute concentrations in the intergranular aluminium phase are roughly proportional to the magnitude of the maximum solid solubility extension of chromium, manganese and vanadium into the aluminium phase achieved by rapid quenching, i.e. 5 to 6 at % for chromium [15], 6 to 9 at % for manganese [15] and 1.4 to 2 at % for vanadium [15].

As presented in Table II, the alloy composition of the quasicrystalline single phases is approximated to be $Al_{11}Cr_2$, Al_4Mn and Al_4V. The solute concentration of Al–Cr quasicrystal is lower by 4.6% than that of Al–Mn and Al–V quasicrystals. It is thus

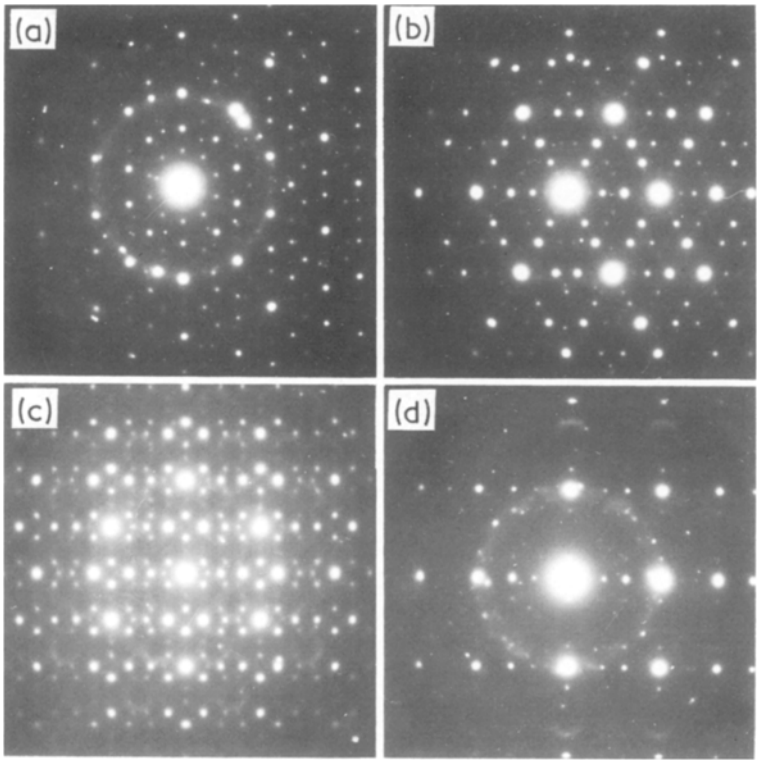

Figure 3 Selected area electron diffraction patterns of a rapidly quenched $Al_{85.5}Cr_{14.5}$ alloy. (a) $(1\,0\,0\,0\,0\,0)_q$, (b) $(1\,1\,1\,0\,0\,0)_q$, (c) $(1\,1\,0\,0\,0\,0)_q$, and (d) $(1\,1\,2\,0\,0\,0)_q$.

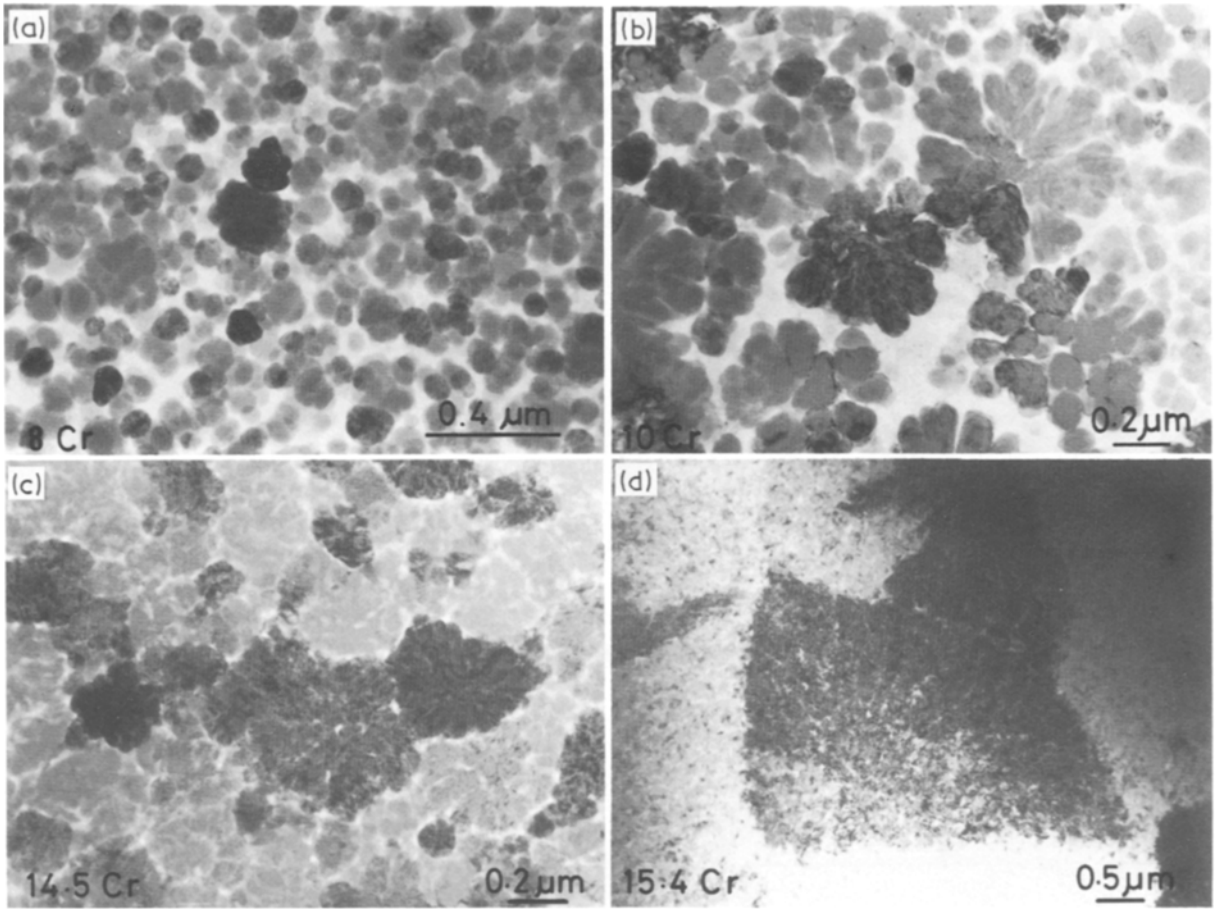

Figure 4 Bright-field electron micrographs of rapidly quenched $Al_{92}Cr_8$ (a), $Al_{90}Cr_{10}$ (b), $Al_{85.5}Cr_{14.5}$ (c) and $Al_{84.6}Cr_{15.4}$ (d) alloys.

concluded that the solute concentration required to form a quasicrystalline single phase is not always constant even in the same aluminium-base alloy system. Very recently, a structure model including the three-dimensional configuration of aluminium and solute atoms in the icosahedral quasicrystals has been proposed [8]; the quasicrystal is composed of two types of basic golden rhombohedra, acute and obtuse ones, consisting of aluminium and manganese atoms. The proposal was made by fitting the observed high-resolution electron microscopic images with the projections of a three-dimensional space filling of the Penrose type skeleton which had recently been completed by Ogawa [16]. The resulting atomic ratio of solute atom to aluminium in the structure model is 20%, in good agreement with the observed results of Al–Mn and Al–V quasicrystals. However, the analytical atomic ratio of Al–Cr quasicrystal is about 15.4% which is lower by about 4.5% than the value expected from the structure model. Such a deviation suggests the possibility that the chromium site in the two types of basic golden rhombohedra can be partially replaced by aluminium atoms in the range less than about 4 to 5%. The reason why only chromium atoms can replace aluminium atoms remains unknown within the present study. A series of investigations on the quasicrystals of Al–X alloys containing solute atoms other than manganese, vanadium or chromium will shed some light on a more systematic interpretation of the formation of quasicrystals at different solute concentrations.

3.2. Formation of a metastable crystalline phase

In some electron diffraction patterns taken from rapidly quenched $Al_{84.6}Cr_{15.4}$ alloy, extra reflection spots which appear to possess five-, three- and two-fold symmetries are observed, in addition to the regular spots of the quasicrystalline phase, as exemplified in Figs 7a to d. It can be seen that the interlattice spacings estimated from the extra spots are larger by about 10 to 12% than that of the quasicrystalline phase. Furthermore, the bright field image (Fig. 8c) taken at remarkably magnified condition reveals the occurrence of the moiré fringes which are distributed homogeneously over the micrograph. The spacing of the moiré fringes is not always constant, and is in the range from about 0.5 to 8 nm. The spacing of moiré fringes caused by the difference in lattice spacing of the electron diffraction pattern shown in Fig. 8b is estimated to be 2.1 nm for the parallel moiré and 0.5 to 2.1 nm for the rotation moiré, being in the same order as the actually observed spacings ($\simeq$0.5 to 8 nm). Thus, the occurrence of the moiré fringe and the good correspondence of the observed fringe spacings with the calculated ones indicate that a metastable phase with a structure similar to the quasicrystalline phase is formed in $Al_{84.6}Cr_{15.4}$ alloy by rapid solidification. Although the details of structure of the metastable phase remain unknown within the present study, it is important to point out that the metastable phase is in good accordance with an intermediate phase which appears in the annealing-induced

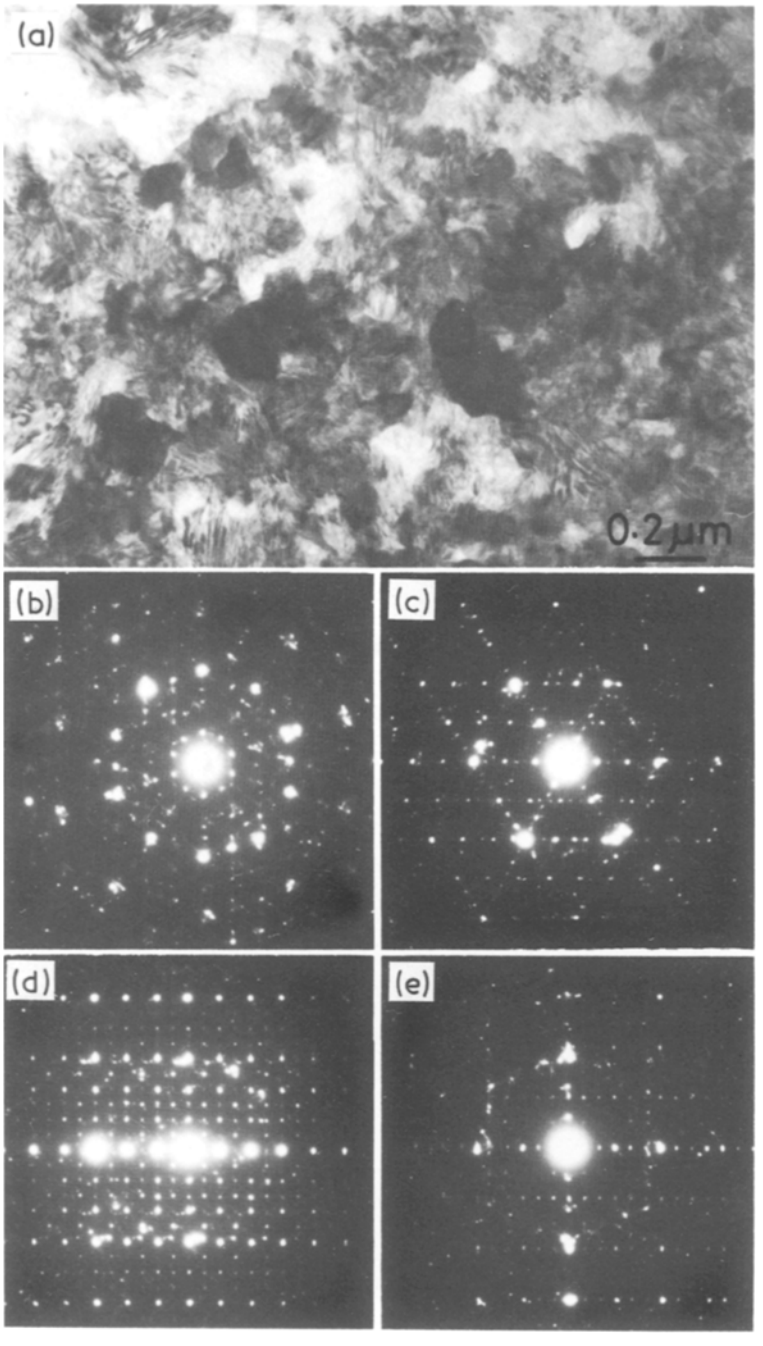

Figure 5 Bright-field electron micrograph (a) and selected area diffraction patterns (b–e) of a rapidly quenched $Al_{83.5}Cr_{16.5}$ alloy.

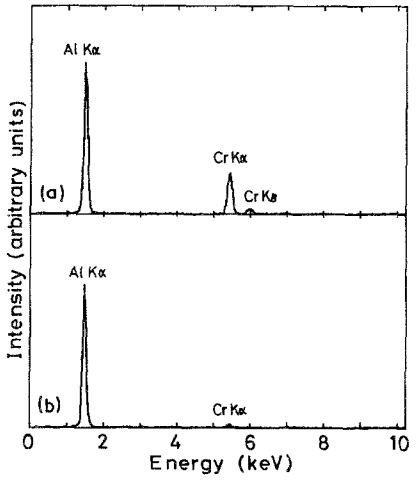

Figure 6 Energy dispersive X-ray spectra of a rapidly quenched $Al_{90}Cr_{10}$ alloy. (a) Transgranular quasicrystalline phase and (b) intergranular aluminium phase.

transition from the quasicrystalline phase to stable orthorhombic $Al_{11}Cr_2$ compound for rapidly quenched $Al_{84.6}Cr_{15.4}$ alloy.

3.3. Electrical resistivity and hardness

Fig. 9 shows the change in electrical resistivity at room temperature ($\varrho_{R.T.}$) as a function of chromium concentration for rapidly quenched Al–Cr alloys, together with the data of rapidly quenched Al–Mn alloys [11]. The $\varrho_{R.T.}$ value of the Al–Cr alloys is 0.50 $\mu\Omega$m at 10% Cr, increases gradually with increasing chromium content and rapidly at compositions above 14.5% Cr and reaches 2.72 $\mu\Omega$m for $Al_{84.6}Cr_{15.4}$ alloy with quasicrystal single phase. The ϱ values of the Al–Cr quasicrystal are considerably lower than those of the Al–Mn quasicrystal. Fig. 10 shows the temperature dependence of ϱ of the $Al_{84.6}Cr_{15.4}$ quasicrystal, along with the data of annealed $Al_{84.6}Cr_{15.4}$ alloy with the stable $Al_{11}Cr_2$

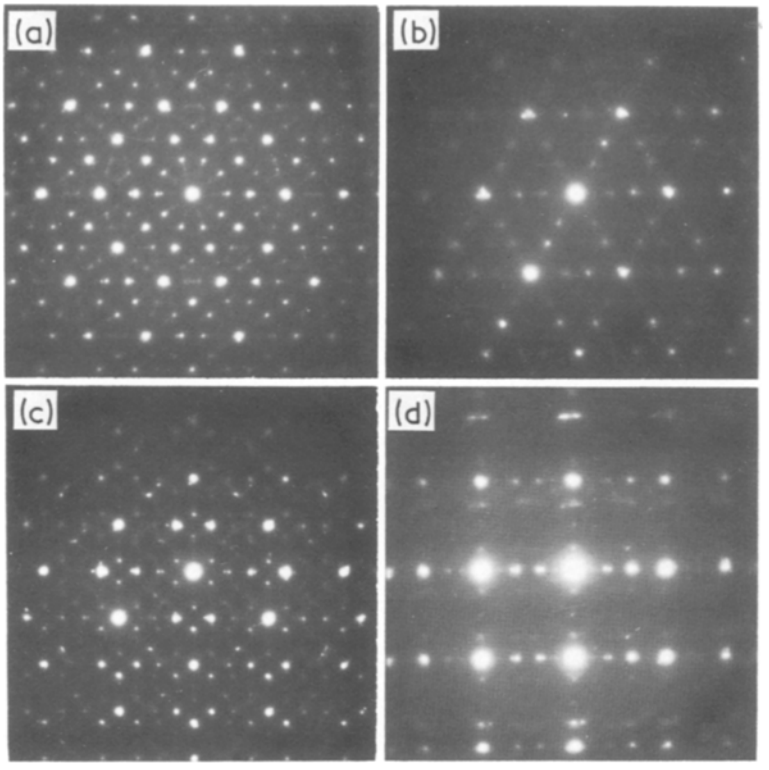

Figure 7 Selected area electron diffraction patterns of a rapidly quenched $Al_{84.6}Cr_{15.4}$ alloy. (a) $(100000)_q$, (b) $(111000)_q$, (c) $(110000)_q$, and (d) $(112000)_q$.

compound phase. The ϱ remains almost constant below about 25 K and increases almost linearly in the higher temperature range. No linear increase of ϱ with lowering temperature in the range below about 60 K, observed for the $Al_{77.5}Mn_{22.5}$ quasicrystal [9, 10], is seen for the Al–Cr quasicrystal. Furthermore, the structural transition from quasicrystal to stable compound causes a decrease of ϱ by 18 to 28% and a disappearance of the plateau stage at temperatures below 25 K, indicating that electrical resistive behaviour at low temperatures is different for the quasicrystal and the stable $Al_{11}Cr_2$ compounds. The temperature coefficient of resistivity at 293 K, $1/\varrho_{293}(d\varrho/dT)$, for $Al_{84.6}Cr_{15.4}$ alloy, is $4.74 \times 10^{-4}\,K^{-1}$ for the quasicrystal and increases to $7.55 \times 10^{-4}\,K^{-1}$ upon the structural charge into the stable compound.

The Vickers hardness (H_v) of rapidly quenched Al–Cr alloys exhibits a compositional dependence similar to that for the ϱ values as plotted in Fig. 11. H_v is about 255 DPN for $Al_{90}Cr_{10}$, increases gradually with increase in chromium and rapidly at compositions above 14.5 at % Cr and reaches about 710 DPN for $Al_{84.6}Cr_{15.4}$. The hardness value of the Al–Cr quasicrystal is lower by 300 DPN than that ($\simeq$ 1010 DPN) for $Al_{77.5}Mn_{22.5}$ quasicrystal. Finally it is seen in Figs 9 and 11 that the rapid increases of ϱ and H_v are accompanied by the disappearance of the aluminium phase.

3.4. Thermal stability and decomposition behaviour

Fig. 12 shows DSC curves obtained at a heating rate of $40\,K\,min^{-1}$ for rapidly quenched $Al_{100-x}Cr_x$ (x = 8, 10, 14.5 and 15.4 at %) alloys. Additionally, the onset transformation temperature (T_t) at which the quasicrystalline phase begins to decompose accom-

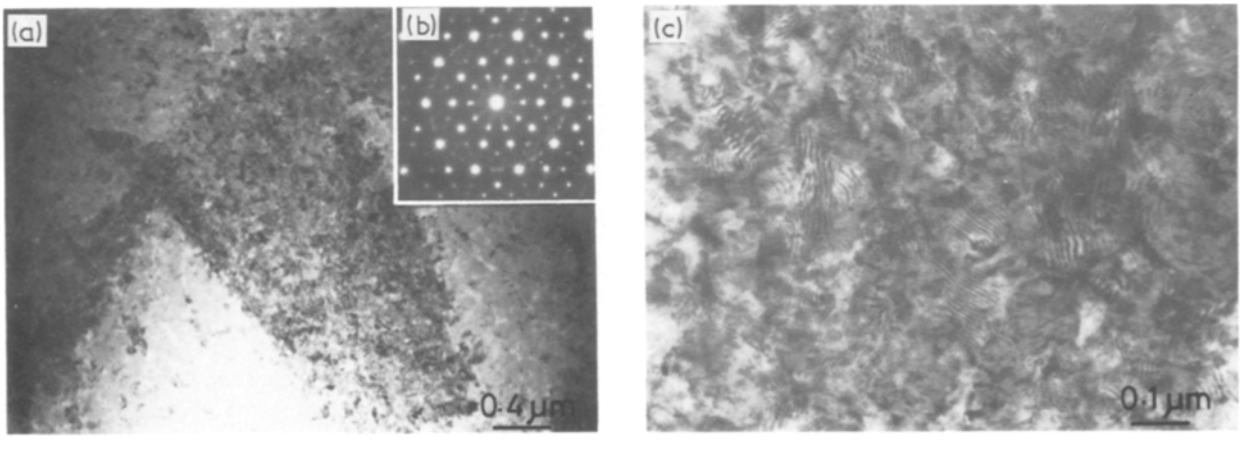

Figure 8 Bright-field electron micrographs (a and c) and selected area diffraction pattern (b) of a rapidly quenched $Al_{84.6}Cr_{15.4}$ alloy. The micrograph (c) is a highly magnified structure of the same region as (a).

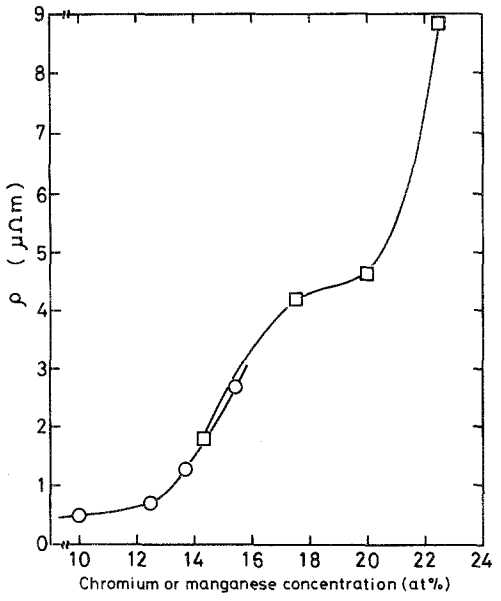

Figure 9 Electrical resistivity of rapidly quenched Al–Cr alloys as a function of chromium content at 293 K. The data of rapidly quenched Al–Mn alloys are also shown for comparison. ○, Al–Cr; □, Al–Mn alloys.

panied by exothermic peak and the heat of transformation (ΔH_t) are plotted as a function of chromium content in Fig. 13. T_t and ΔH_t are 602 K and 790 J mol^{-1} K^{-1} at 8% Cr, increase continuously with increase in chromium content and show maximum values of 644 K and 1805 J mol^{-1} K^{-1} at 14.5% Cr. The further increase in chromium content to 15.4% Cr results in decreases of T_t to 625 K and ΔH_t to 550 J mol^{-1}. Although the thermal stability of the icosahedral phase tends to increase with increasing chromium content from 6 to 14.5% Cr, $Al_{84.6}Cr_{15.4}$ quasicrystalline single phase exhibits T_t and ΔH_t much smaller than those of $Al_{85.5}Cr_{14.5}$ alloys. The marked deflection of T_t and ΔH_t between 14.5 and 15.4 at % Cr is thought to be attributed to a distinct difference of decomposition behaviour as described below; Al + quasicrystal → Al + equilibrium compound for $Al_{85.5}Cr_{14.5}$ and quasicrystal → metastable intermediate phase (T phase) → stable $Al_{11}Cr_2$ compound for $Al_{84.6}Cr_{15.4}$.

In order to assess the change in thermal energy state of the quasicrystal upon heating up to a temperature (600 K) below the onset transformation temperature, the temperature dependence of specific heat (C_p) of

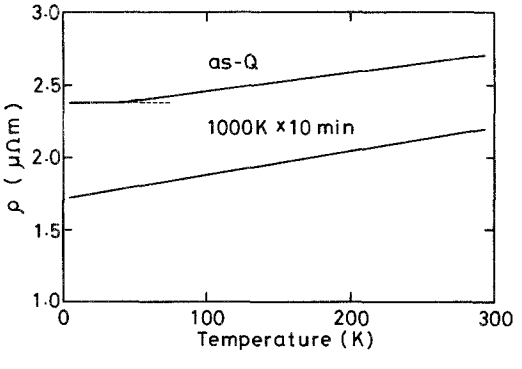

Figure 10 Electrical resistivity of a rapidly quenched $Al_{84.6}Cr_{15.4}$ alloy as a function of temperature. The data of $Al_{84.6}Cr_{15.4}$ alloy annealed for 10 min at 1000 K are also shown for comparison.

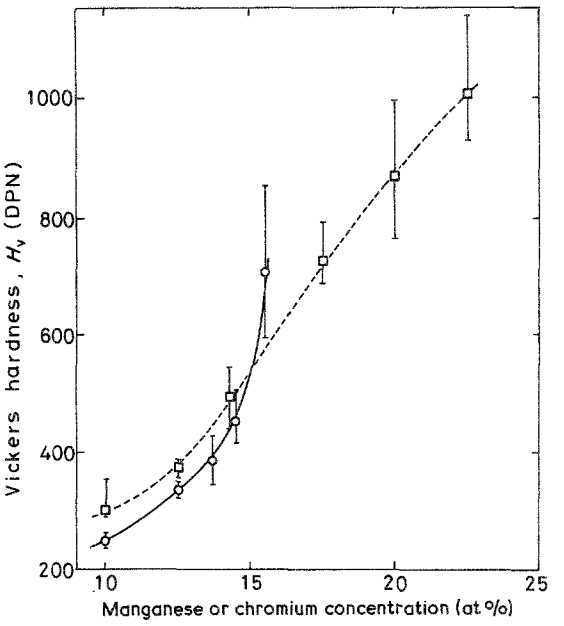

Figure 11 Vickers hardness of rapidly quenched Al–Cr alloys as a function of chromium content. The data of rapidly quenched Al–Mn alloys are also shown for comparison. Load: 25 g. ○, Al–Cr; □, Al–Mn.

rapidly quenched $Al_{84.6}Cr_{15.4}$ alloy with quasicrystalline single phase was examined with a differential scanning calorimeter. Fig. 14 shows the thermograms of the quasicrystalline Al–Cr alloy in as-quenched and annealed (600 K for 1 min) states, along with the data of equilibrium $Al_{11}Cr_2$ compound with an orthorhombic structure obtained upon annealing at 800 K for 1 h. The C_p value of the as-quenched quasicrystal is about 26.2 J mol^{-1} K^{-1} near room temperature. As the temperature rises, the C_p value increases gradually by the increase in the ease of thermal vibration of atoms, but the increase of $C_p(T)$ becomes smaller at temperatures above 440 K. Considering the result that no distinct change in X-ray diffraction pattern is observed before and after annealing at 600 K for 10 min, the difference in the $C_p(T)$ values between the

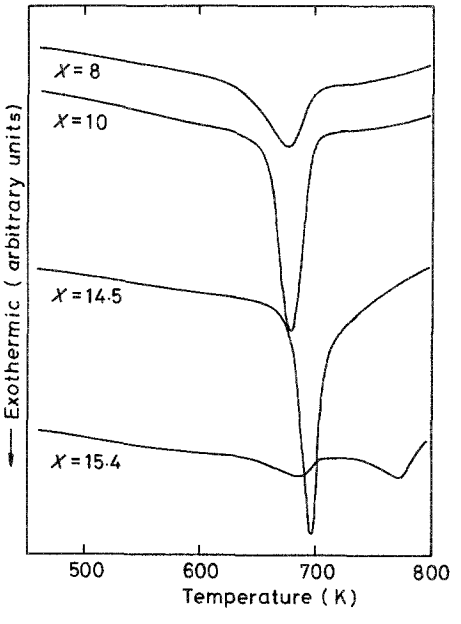

Figure 12 Differential scanning calorimetry curves for rapidly quenched $Al_{100-x}Cr_x$ (x = 8, 10, 14.5 and 15.4 at %) alloys.

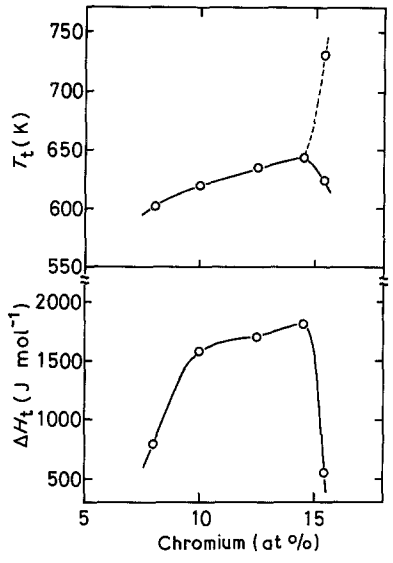

Figure 13 Changes in the onset transformation temperature from the quasicrystal to crystalline phase, T_t, and the heat of transformation, ΔH_t, as a function of chromium content for rapidly quenched Al–Cr alloys.

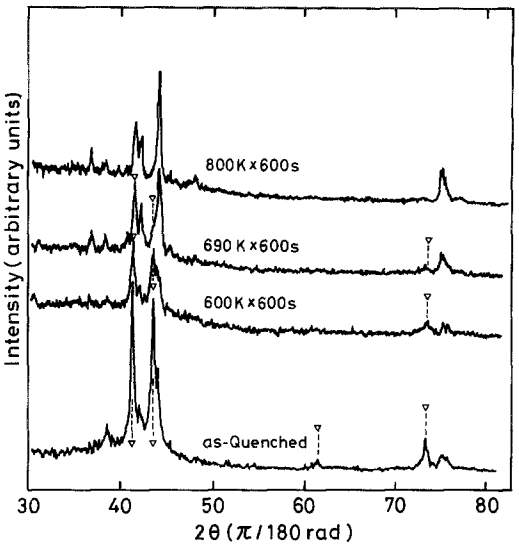

Figure 15 Change in X-ray diffraction patterns of quasicrystalline $Al_{84.6}Cr_{15.4}$ alloy upon annealing in vacuum for 10 min at 600, 690 and 800 K. ▽, Quasicrystalline phase.

as-quenched and the annealed samples, i.e., the occurrence of the irreversible broad exothermic peak accompanied by a heat of about 151 J mol^{-1}, is believed to result from the heating-induced irreversible structural change probably due to the annihilation of various kinds of quenched-in 'defects'. Furthermore, it can be seen that the C_p values in the whole temperature range are consistently higher by about 0.2 to 0.5 J mol^{-1} K^{-1} for the quasicrystal sample than for the stable orthorhombic $Al_{11}Cr_2$. The decrease in $C_p(T)$ is attributed to the structural change from the nonequilibrium quasicrystalline structure with higher atomic configuration energy to the equilibrium orthorhombic structure with lower configuration energy. Fig. 14 also shows that the temperature dependence of vibrational specific heat is larger by about 10% for the quasicrystalline phase than for the orthorhombic phase. Such a difference allows us to infer that the quasicrystalline phase possesses a lower packing density as compared with that of the equilibrium $Al_{11}Cr_2$ compound. This inference is consistent with the previous experimental results [4, 5] that the density of Al–Mn quasicrystal increases by about 1.5% upon the structural change from the quasicrystal to the stable phase.

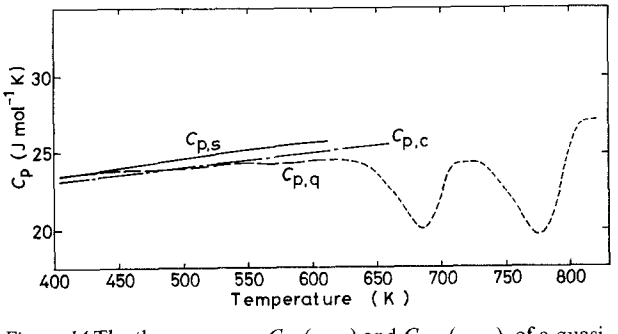

Figure 14 The thermograms, $C_{p,q}$(– – –) and $C_{p,s}$, (——), of a quasicrystalline $Al_{84.6}Cr_{15.4}$ alloy in as-quenched and annealed (600 K × 1 min states (40 K min^{-1}). The thermogram $C_{p,c}$ (–·–·–) of an orthorhombic $Al_{84.6}Cr_{15.4}$ alloy obtained by annealing the quasicrystal at 800 K for 1 h was also presented for comparison.

Structural change corresponding to the appearance of the two exothermic peaks for $Al_{84.6}Cr_{15.4}$ quasicrystal shown in Fig. 13 was examined by transmission electron microscopy and X-ray diffraction analysis. Fig. 15 shows the change in X-ray diffraction patterns of quasicrystalline $Al_{84.6}Cr_{15.4}$ alloy upon annealing for 10 min at 600, 690 and 800 K. As is apparent from Fig. 12, the three annealing temperatures (T_a) correspond to the temperatures below the first exothermic peak and below and above the second peak, respectively. As shown in Fig. 15, the diffraction peaks of the quasicrystal remain almost unchanged at T_a = 600 K, but the annealing at 690 K results in almost complete disappearance of the quasicrystalline peaks and appearance of a metastable intermediate phase with a structure similar to the icosahedral phase. The further rise of T_a to 800 K causes a change from the intermediate phase to stable orthorhombic $Al_{11}Cr_2$ compound. Fig. 16 shows the changes in bright field images and selected area diffraction patterns of $Al_{84.6}Cr_{15.4}$ quasicrystal with T_a. The Al–Cr alloy consists of quasicrystal and metastable intermediate phases after annealing at 600 K for 10 min, mostly the intermediate phases after annealing at 600 K for 10 min and stable $Al_{11}Cr_2$ compound after annealing at 800 K for 10 min. The two-stage decomposition behaviour is in accordance with the results obtained by X-ray diffraction analysis and DSC curves. Accordingly, the two exothermic peaks for $Al_{84.6}Cr_{15.4}$ quasicrystal are attributed to the transitions from quasicrystal to metastable intermediate phase and from the intermediate phase to stable orthorhombic compound. The similar two-stage decomposition behaviour has also been recognized for $Al_{80}Mn_{20}$ quasicrystalline single phase in which the decomposition occurs in the process of quasicrystal → a metastable intermediate phase (T phase) → hexagonal Al_4Mn [17].

On the other hand, bright field electron micrographs and selected area diffraction patterns of $Al_{85.5}Cr_{14.5}$ alloy annealed at temperatures above the onset transition temperature are completely different

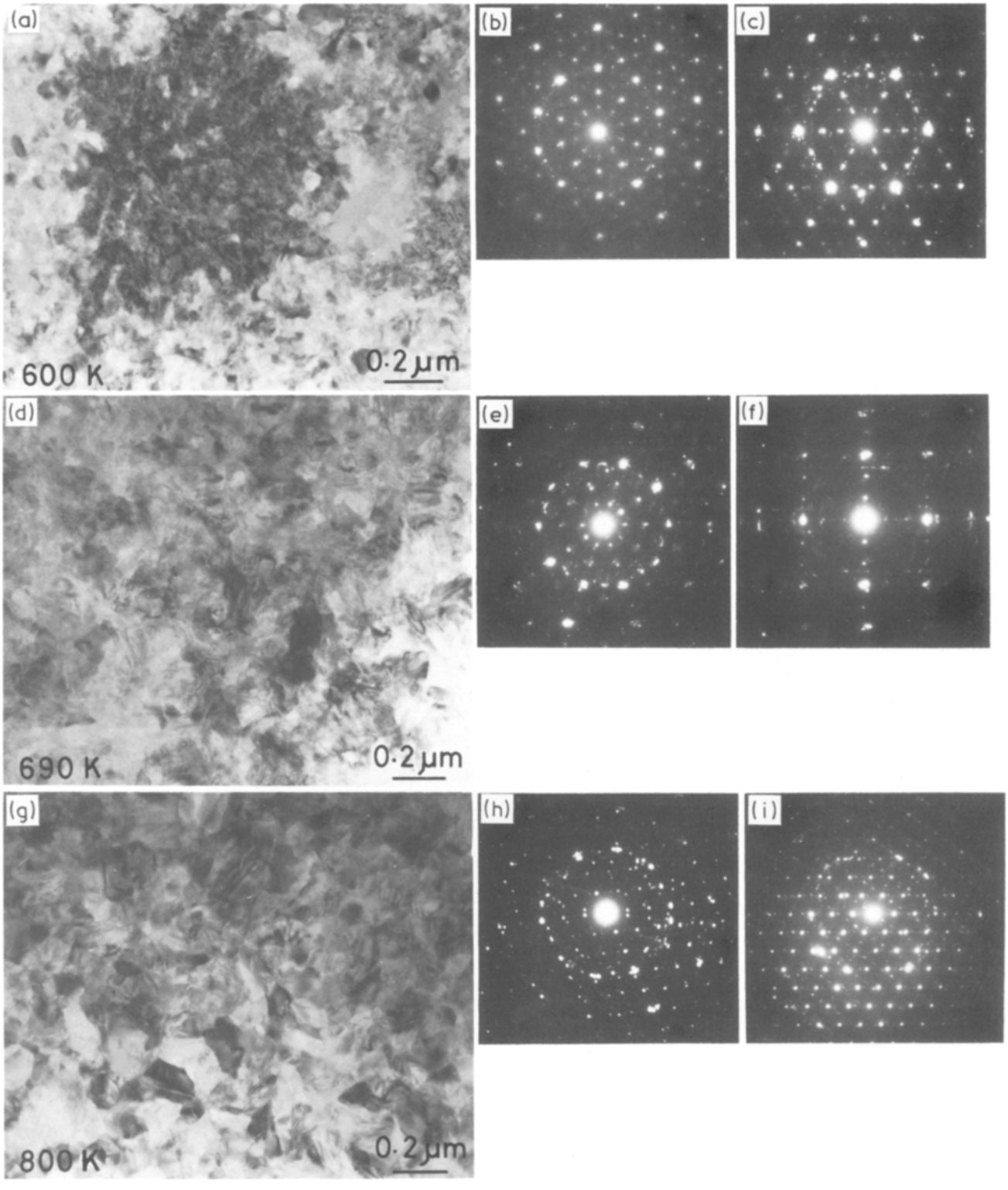

Figure 16 Bright-field electron micrographs and selected area diffraction patterns of $Al_{84.6}Cr_{15.4}$ alloy annealed at 600 K (a–c), 690 K (d–f) and 800 K (g–i) for 10 min after rapid quenching.

from the as-quenched quasicrystal and the structure was identified to be mainly composed of Al–Cr compounds. No quasicrystalline and metastable intermediate phases are seen for the $Al_{85.5}Cr_{14.5}$ samples after annealing at temperatures above the onset decomposition temperature. From these results, it is concluded that the high intensity exothermic peak for Al–Cr alloys below about 15% Cr is due to the structural change from quasicrystal + Al to stable phases (Al + Al_7Cr and Al_7Cr + $Al_{11}Cr_2$). This decomposition behaviour is largely different from that of $Al_{84.6}Cr_{15.4}$ quasicrystalline single phase and this difference is thought to cause the distinctly distinguishable deflection in the T_t and ΔH_t at a composition between 14.5 and 15.4% Cr.

4. Summary

The structure of rapidly solidified Al–Cr alloys is composed of quasicrystal and fcc aluminium phases at compositions below about 15 at % Cr and a quasi-

crystal single phase with a grain size of 2 to 3 μm in the vicinity of 15.4 at % Cr. The further increase in chromium content results in a mixed structure of crystalline compounds. Analytical solute concentration in the quasicrystalline phase is not always constant and increases continuously in the range from 9.0 to 15.4 at % Cr with increasing nominal solute concentration from 6 to 15.4 at % Cr. The quasicrystal in rapidly quenched Al–Cr alloys can be thus approximated to be $Al_{11}Cr_2$ with a maximum deviation of about 6 at % Cr from the stoichiometric ratio to lower concentration side. Vickers hardness and electrical resistivity increase gradually with increasing chromium content and drastically above about 14.5 at % Cr at which the crystalline aluminium phase almost disappears. These are 710 DPN, 2.38 $\mu\Omega$m at 4.2 K and 2.72 $\mu\Omega$m at 293 K for $Al_{84.6}Cr_{15.4}$ with quasicrystalline single phase. The onset transformation temperature of quasicrystal to crystalline phases, T_t, and the heat of transformation, ΔH_t, show maximum values of 644 K and 1805 J mol^{-1} at 14.5 at % Cr and decrease to 625 K and 550 J mol^{-1} at 15.4 at % Cr. The decrease in thermal stability for the quasicrystalline single phase is interpreted as due to the difference of decomposition behaviour; the quasicrystal in $Al_{84.6}Cr_{15.4}$ decomposes in the processes of quasicrystal → quasicrystal + metastable intermediate crystalline phase → stable orthorhombic $Al_{11}Cr_2$, while the quasicrystal + Al structure in Al–Cr alloys containing 6 to 14.5 at % Cr changes directly to stable phases of Al + Al_7Cr and Al_7Cr + $Al_{11}Cr_2$.

Acknowledgements

The authors are sincerely grateful to Mr M. Kikuchi of The Research Institute for Iron, Steel and Other Metals, Tohoku University, for obtaining the EDX spectra.

References

1. K. SCHECHTMAN, I. A. BLECH, D. GRATIAS and J. W. CAHN, *Phys. Rev. Lett.* **53** (1984) 1951.
2. K. HIRAGA, M. HIRABAYASHI, A. INOUE and T. MASUMOTO, *Sci. Rep. Res. Inst. Tohoku Univ.* **A32** (1985) 309.
3. D. SCHECHTMAN and I. A. BLECH, *Met. Trans.* **16A** (1985) 1005.
4. H. S. CHEN, C. H. CHEN, A. INOUE and J. T. KRAUSE, *Phys. Rev. B* **32** (1985) 1940.
5. K. F. KELTON and T. W. WU, *Appl. Phys. Lett.* **46** (1985) 1059.
6. P. A. BANCEL, P. A. HEINEY, P. W. STEPHENS, A. I. GOLDMAN and P. M. HORN, *Phys. Rev. Lett.* **54** (1985) 2422.
7. K. KIMURA, T. HASHIMOTO, K. SUZUKI, K. NAGAYAMA, H. INO and S. TAKEUCHI, *J. Phys. Soc. Jpn* **54** (1985) 3217.
8. K. HIRAGA, M. HIRABAYASHI, A. INOUE and T. MASUMOTO, *ibid.* **54** (1985) 4077.
9. T. MASUMOTO, A. INOUE, M. OGUCHI, K. FUKAMICHI, K. HIRAGA and M. HIRABAYASHI, *Trans. Jpn Inst. Metals* **27** (1986) 81.
10. K. FUKAMICHI, T. MASUMOTO, M. OGUCHI, A. INOUE, T. GOTO, T. SAKAKIBARA and S. TODO, *J. Phys. F, Metal Phys.* **16** (1986) 1059.
11. A. INOUE, L. ARNBERG, B. LEHTINEN, M. OGUCHI and T. MASUMOTO, *Met. Trans.* **17A** (1986) 1657.
12. K. V. RAO, J. FILDER and H. S. CHEN, *Europhys. Lett.* **1** (1986) 647.
13. H. YOSHIDA, *Bull. Jpn Inst. Metals* **21** (1982) 925.
14. J. J. HREN, J. I. GOLDSTEIN and D. C. JOY (eds), in Introduction to Analytical Electron Microscopy, Plenum Press, New York, 1979.
15. H. JONES, *Aluminum* **54** (1978) 274.
16. T. OGAWA, *J. Phys. Soc. Jpn* **54** (1985) 3205.
17. K. KIMURA, T. HASHIMOTO, K. SUZUKI, K. NAGAYAMA, H. INO and S. TAKEUCHI, *J. Pys. Soc. Jpn* **55** (1986) 534.

Received 24 June
and accepted 9 September 1986